

RESEARCH ARTICLE

Targeted Deletion of *Btg1* and *Btg2* Results in Homeotic Transformation of the Axial Skeleton

Esther Tijchon¹, Dorette van Ingen Schenau¹, Fred van Opzeeland², Felice Tirone³, Peter M. Hoogerbrugge⁴, Frank N. Van Leeuwen¹, Blanca Scheijen^{1*}

1 Laboratory of Pediatric Oncology, Radboud university medical center, Nijmegen, The Netherlands, **2** Laboratory of Pediatric Infectious Diseases, Radboud university medical center, Nijmegen, The Netherlands, **3** Institute of Cell Biology and Neurobiology, National Research Council, Fondazione Santa Lucia 00143, Rome, Italy, **4** Princess Maxima Center for Pediatric Oncology, Utrecht, The Netherlands

☞ These authors contributed equally to this work.

* Blanca.Scheijen@radboudumc.nl



OPEN ACCESS

Citation: Tijchon E, van Ingen Schenau D, van Opzeeland F, Tirone F, Hoogerbrugge PM, Van Leeuwen FN, et al. (2015) Targeted Deletion of *Btg1* and *Btg2* Results in Homeotic Transformation of the Axial Skeleton. *PLoS ONE* 10(7): e0131481. doi:10.1371/journal.pone.0131481

Editor: Tim Thomas, The Walter and Eliza Hall of Medical Research, AUSTRALIA

Received: March 6, 2015

Accepted: June 1, 2015

Published: July 28, 2015

Copyright: © 2015 Tijchon et al. This is an open access article distributed under the terms of the [Creative Commons Attribution License](https://creativecommons.org/licenses/by/4.0/), which permits unrestricted use, distribution, and reproduction in any medium, provided the original author and source are credited.

Data Availability Statement: All relevant data are contained within the paper.

Funding: Funding provided by Stichting Kinderen Kankervrij (KiKA) grant-77; <https://www.kika.nl/?gclid=CMW-652BIMQCF57MtAod1H8AzA>. The funders had no role in study design, data collection and analysis, decision to publish, or preparation of the manuscript.

Competing Interests: The authors have declared that no competing interests exist.

Abstract

Btg1 and *Btg2* encode highly homologous proteins that are broadly expressed in different cell lineages, and have been implicated in different types of cancer. *Btg1* and *Btg2* have been shown to modulate the function of different transcriptional regulators, including Hox and Smad transcription factors. In this study, we examined the *in vivo* role of the mouse *Btg1* and *Btg2* genes in specifying the regional identity of the axial skeleton. Therefore, we examined the phenotype of *Btg1* and *Btg2* single knockout mice, as well as novel generated *Btg1*^{-/-};*Btg2*^{-/-} double knockout mice, which were viable, but displayed a non-mendelian inheritance and smaller litter size. We observed both unique and overlapping phenotypes reminiscent of homeotic transformation along the anterior-posterior axis in the single and combined *Btg1* and *Btg2* knockout animals. Both *Btg1*^{-/-} and *Btg2*^{-/-} mice displayed partial posterior transformation of the seventh cervical vertebra, which was more pronounced in *Btg1*^{-/-};*Btg2*^{-/-} mice, demonstrating that *Btg1* and *Btg2* act in synergy. Loss of *Btg2*, but not *Btg1*, was sufficient for complete posterior transformation of the thirteenth thoracic vertebra to the first lumbar vertebra. Moreover, *Btg2*^{-/-} animals displayed complete posterior transformation of the sixth lumbar vertebra to the first sacral vertebra, which was only partially present at a low frequency in *Btg1*^{-/-} mice. The *Btg1*^{-/-};*Btg2*^{-/-} animals showed an even stronger phenotype, with L5 to S1 transformation. Together, these data show that both *Btg1* and *Btg2* are required for normal vertebral patterning of the axial skeleton, but each gene contributes differently in specifying the identity along the anterior-posterior axis of the skeleton.

Introduction

The vertebrate axial skeleton is comprised of similar structures that extend from anterior to posterior along the body axis: the occipital skull bones, cervical, thoracic, lumbar, sacral and

caudal vertebrae. In mice, there are 30 precaudal vertebrae distributed into seven cervical, thirteen thoracic, six lumbar and four sacral vertebrae [1]. Vertebral development involves two phases, an early stage of somite segmentation from the presomitic mesoderm (PSM) and a later stage of somatic patterning and specification [2]. Segmental identity of the axial skeleton is regulated by a variety of signaling mechanisms and requires the local activation of specific transcriptional regulators, known as Hox genes. This gene family comprises 39 highly conserved transcription factors that are organized into four clusters, including *HoxA*, *HoxB*, *HoxC* and *HoxD* [3, 4]. *Hox* genes are expressed in gradients along the anterior-posterior axis of the body [5–7], and as such control the identity of the axial skeleton. Deregulation of *Hox* gene function leads to homeotic transformations, in which one structure acquires the morphological characteristics of an adjacent homologous structure, a phenotype dictated by the cluster of *Hox* genes that is affected [8, 9]. Other transcriptional regulators important for proper control of vertebral identities include the mammalian Trithorax group (TrxG) and Polycomb group (PcG) proteins, which control the expression of *Hox* genes [10, 11]. Moreover, Hox gene expression is regulated by different signaling pathways, including bone morphogenetic protein (BMP), which is required for normal axial skeletal development [12, 13].

The *B cell translocation gene 1* (*Btg1*) and *Btg2* belong to the BTG/TOB family of anti-proliferation genes, and their gene products share 74% protein sequence similarity [14, 15]. *Btg1* and *Btg2* proteins regulate various cellular processes including proliferation, differentiation and apoptosis, while deregulated expression has been observed in various cancers, including B cell malignancies [16–19]. In addition, the *BTG1* gene is frequently affected by monoallelic deletions in pediatric B-cell precursor acute lymphoblastic leukemia (BCP-ALL), while this has not been observed for *BTG2* [18, 20]. On the other hand, both genes are targeted by point mutations in diffuse large B cell lymphomas [21, 22]. Furthermore, both proteins enhance the transcriptional activity of the homeodomain protein HoxB9, whereas *Btg2* was shown to associate with receptor regulated SMAD proteins SMAD1 and SMAD8, thereby activating BMP-dependent transcription [23, 24]. Previous studies using *Btg2*^{-/-} mice revealed posterior homeotic transformations of axial skeleton vertebrae, which has been attributed to impaired BMP/Smad signaling [23]. However, it remains to be established whether *Btg1* regulates patterning of axial vertebrae and displays similar functions as *Btg2*.

Several classes of leukemia-associated genes, including Hox transcription factors and their upstream regulator *Bmi1*, play a critical role in regional patterning of the vertebrate body plan [8, 25–27]. Here, we examined the *in vivo* role of *Btg1* and *Btg2* in specifying the regional identity of vertebrae along the anterior-posterior axis of the skeleton using both single and double knockout mice for *Btg1* and *Btg2*. This analysis revealed that both *Btg1* and *Btg2* regulate vertebra specification at the cervical-thoracic and lumbar-sacral junction. On the other hand, *Btg2* fulfills a unique role in patterning of the thoracic-lumbar junction, which is not affected in the *Btg1*^{-/-} mice.

Methods

Experimental Animals

C57BL/6J *Btg1*^{-/-} and *Btg2*^{-/-} mice have been described earlier [28] and were a kind gift of J.P. Rouault and F. Tirone respectively. [23]. *Btg1*^{-/-};*Btg2*^{-/-} mice were obtained by multiple intercrossing of *Btg1*^{-/-} with *Btg2*^{-/-} mice. Animals were maintained under specific pathogen-free conditions at our animal facility. All animal experiments were approved by the Animal Experimental Committee of the Radboud university medical center and were performed in accordance with institutional and national guidelines.

Genotyping of mice was routinely performed by PCR, using DNA derived from ear clips. To identify mice carrying either null or wild-type alleles, two primers complementary to the targeted exon 1 (*mBtg1_F* 5'-CCATGCATCCCTTCTACACCC-3'; *mBtg1_R* 5'-TGCAGGCTCTGGCTGAAAGT-3') and one primer complementary to the neomycin cassette (*mBtg1_Neo_R* 5'-CGGAGAACCTGCGTGCAATC-3') were combined. The wild-type (WT) non-targeted *Btg1* allele was identified as a 136bp PCR fragment with the exon 1 primers, and the *Btg1*^{-/-} allele as a 360bp PCR fragment with neomycin specific primer. *Btg2* null wild-type alleles were identified by PCR using four primers, two complementary to the targeted exon 2 for detection of the endogenous *Btg2* allele (*mBtg2_F* 5'-CATCCAAAGGTTCTGGCTATC-3'; *mBtg2_R* 5'-GCCATCACATAGTTCTTCGAG-3'), one complementary to the neomycin cassette and one specific for exon 1 (*mBtg2_Neo_F* 5'-CTTCTATCGCCTTCTTGACGAG-3'; *mBtg2_ExI_R* 5'-CCACGGGAAGAGAACCGACAT-3'), which were combined in the PCR reaction. The wild-type (WT) non-targeted *Btg2* allele was identified as a 289bp PCR fragment with the exon 2 primers, and the *Btg2*^{-/-} allele as a 1372bp PCR fragment with the exon 1 and neomycin specific primers.

Skeletal Staining and Analysis

Embryos of day 18.5dpc were eviscerated and fixed in 95% EtOH at 4°C. The skeleton was stained for cartilage in 70% ethanol/5% acetic acid and 5% Alcian Blue (8GX, Sigma Aldrich) (0.4% Alcian Blue in 70% EtOH) and bone by addition of 0.005% Alizarin Red S (Sigma Aldrich) for 24–48 hours at room temperature. Embryos were destained in series of gradual lower concentrations of KOH and increasing concentrations of glycerol, and finally stored in 100% glycerol.

The skeletons were scored for axial transformations by counting the number of sternbrae, vertebrae (cervical, thoracic, lumbar and sacral) and ribs by microscopic analysis.

Results

Generation of *Btg1* and *Btg2* knockout mice

To investigate the function of *Btg1* and *Btg2* during normal development we obtained *Btg1*^{-/-} and *Btg2*^{-/-} single knockout [23, 28], and generated *Btg1*^{-/-};*Btg2*^{-/-} double knockout mice on a *C57Bl/6J* background and examined their appearance for gross abnormalities (Fig 1A and 1B). Genotyping the offspring showed a non-mendelian inheritance pattern for the *Btg1* knockout allele in the single knockout crosses (Table 1), while the *Btg2* knockout allele was strongly underrepresented in the compound crosses (Table 2). The different homozygous knockout animals showed no obvious developmental defects, although the litter size upon interbreeding of the *Btg1*, *Btg2* or *Btg1*;*Btg2* homozygous knockout lines appeared to be smaller compared to WT animals (Fig 1C).

Homeotic transformation of the axial skeleton in the cervical and thoracic region of *Btg1*- and *Btg2*-deficient mice

To establish whether *Btg1* may display distinct or overlapping functions compared to *Btg2* in specifying the regional identity of the axial skeleton [23], we analyzed the skeletal defects of *Btg1* and *Btg2* single knockout, as well as *Btg1*;*Btg2* double knockout embryos at the age of 18.5 days post-coitus (dpc). In total, we examined the skeletons of 18 wild-type, 21 *Btg1*^{-/-}, 20 *Btg2*^{-/-} and 22 *Btg1*^{-/-};*Btg2*^{-/-} animals, which were obtained from three independent breeding pairs.

Inspection of the upper cervical region in the *Btg1*^{-/-}, *Btg2*^{-/-} and *Btg1*^{-/-};*Btg2*^{-/-} animals did not uncover any abnormalities in the structure and shape of the atlas (C1) or axis (C2).

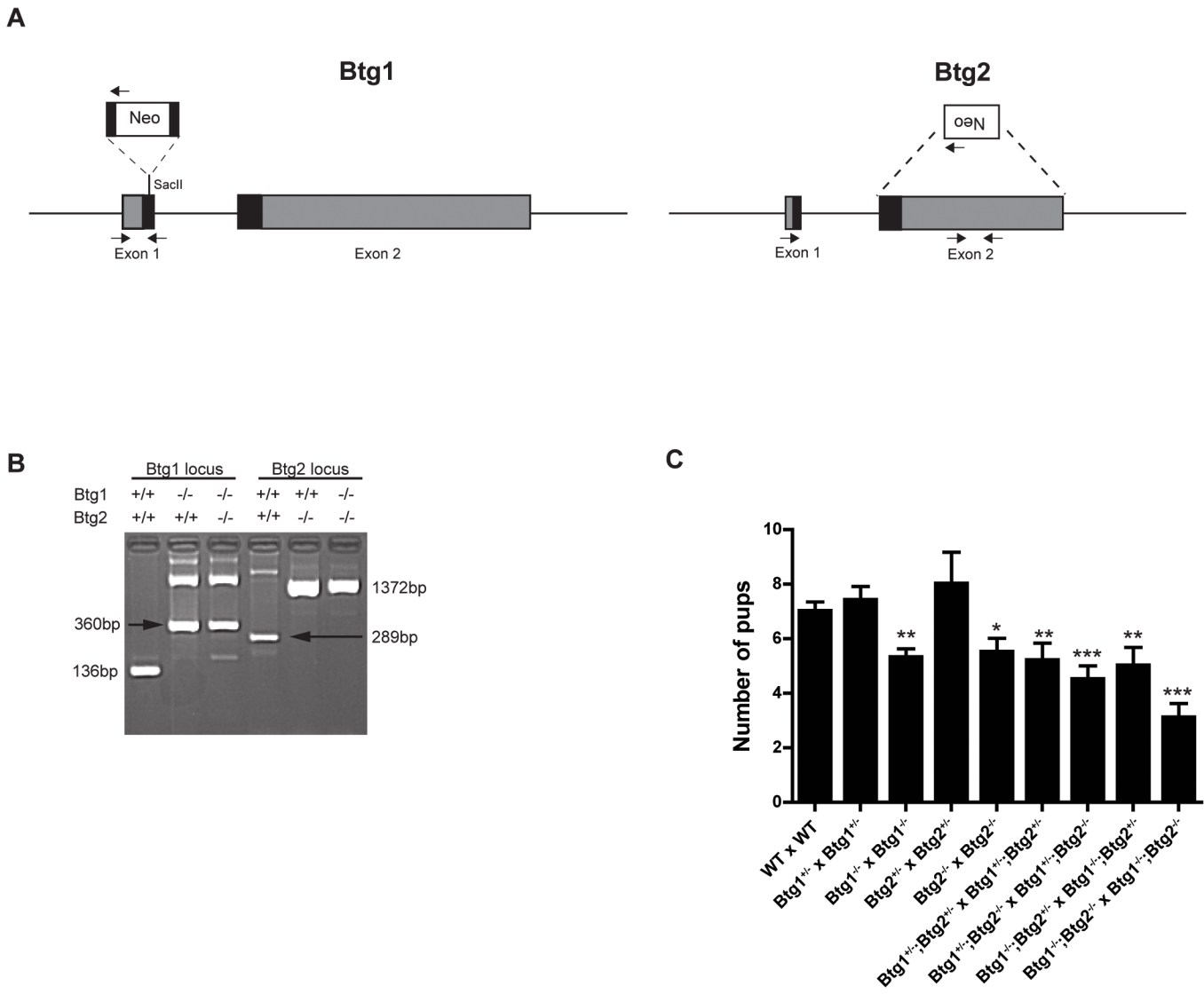


Fig 1. Characterization of *Btg1*^{-/-}, *Btg2*^{-/-} and *Btg1*^{-/-};*Btg2*^{-/-} mice. (A) The mouse *Btg1* gene is disrupted by insertion of a neomycin resistance cassette via *SacII* restriction sites in the first exon. The second exon of the *Btg2* gene is replaced by a neomycin cassette in the antisense direction. The arrows indicate the position of primers used for genotyping. (B) Genotyping of mice was performed by PCR on genomic DNA using primers specific for the *Btg1* and *Btg2* wild-type (WT) and knockout (KO) allele. (C) Number of pups obtained from wild-type, heterozygous and homozygous *Btg1*, *Btg2* and *Btg1**x**Btg2* breedings. Data are from at least 4 independent crossings. *, *P* < 0.05, **, *P* < 0.01, ***, *P* < 0.001.

doi:10.1371/journal.pone.0131481.g001

However, skeletal analysis of the cervical-thoracic junction revealed a common defect among the *Btg1*- and *Btg2*-deficient animals. As expected, most wild-type *C57Bl6/J* mice (72%), showed a small rib anlagen visible as a rudimentary rib attached to the seventh cervical vertebra (C7) (Fig 2A). In contrast, *Btg1*- and *Btg2*-knockout mice displayed a partial or full extensive rib at C7, ranging from 62% in *Btg1*^{-/-}, 35% in *Btg2*^{-/-} and 95% in *Btg1*^{-/-};*Btg2*^{-/-} mice. As a consequence the presence of the rib anlagen on C7 occurred far less frequently in *Btg1*^{-/-} mice (38%) and was almost absent in *Btg1*^{-/-};*Btg2*^{-/-} animals (4.5%) (Table 3). This indicates that in these mice the C7 vertebra acquired the morphological characteristics of the adjacent posterior T1 vertebra, which is therefore termed posterior homeotic transformation. While *Btg1*-deficient mice with a C7 to T1 transformation displayed a fusion of the T1 to the T2 rib without

Table 1. Mendelian inheritance in the offspring of *Btg1*^{-/-}, and *Btg2* single knockout mice.

Breeding pairs	% WT exp./obs.	% +/- exp./obs.	% -/- exp./obs.	P-value
WT x WT	100 / 100	0 / 0	0 / 0	n.s (n = 176)
<i>Btg1</i> ^{+/-} x <i>Btg1</i> ^{+/-}	50 / 71	50 / 29	0 / 0	<0.0001 (n = 24)
<i>Btg1</i> ^{+/-} x <i>Btg1</i> ^{+/-}	25 / 32	50 / 59	25 / 9	0.001 (n = 104)
<i>Btg1</i> ^{+/-} x <i>Btg1</i> ^{-/-}	0 / 0	50 / 56	50 / 44	n.s (n = 126)
<i>Btg1</i> ^{-/-} x <i>Btg1</i> ^{-/-}	0 / 0	0 / 0	100 / 100	n.s (n = 234)
<i>Btg2</i> ^{+/-} x <i>Btg2</i> ^{+/-}	50 / 49	50 / 51	0 / 0	n.s (n = 61)
<i>Btg2</i> ^{+/-} x <i>Btg2</i> ^{+/-}	25 / 30	50 / 54	25 / 16	n.s (n = 32)
<i>Btg2</i> ^{+/-} x <i>Btg2</i> ^{-/-}	0 / 0	50 / 49	50 / 51	n.s (n = 41)
<i>Btg2</i> ^{-/-} x <i>Btg2</i> ^{-/-}	0 / 0	0 / 0	100 / 100	n.s. (n = 177)

Expected (exp.) mendelian inheritance and observed (obs.) inheritance after WT, *Btg1* and *Btg2* breedings. P-values of the mendelian ratios are calculated with the Chi-square test and are either significant if p <0.05 or not significant (n.s).

doi:10.1371/journal.pone.0131481.t001

direct attachment to the sternum (Fig 2B), loss of *Btg2* resulted in both fusion of the T1 to T2 rib as well as direct attachment of the T1 rib to the sternum (Fig 2C). The *Btg1*^{-/-};*Btg2*^{-/-} double knockout mice displayed a more complete and stronger phenotype, where all mice displayed an extra rib at C7, and in 82% of mice the T1 rib was directly attached to the sternum (Fig 2D).

Normally, the first seven pairs of ribs (T1-T7) form sternocostal junctions with the sternum, where five ossified sternebrae can be distinguished as well as the posterior xiphoid process. In the *Btg1*^{-/-} and *Btg2*^{-/-} mice we observed that in about 5% of the animals the T7 rib at one side was not attached to the sternum. However, a more severe phenotype was observed in the *Btg1*^{-/-};*Btg2*^{-/-} mice, where 36% of the animals displayed attachment of T7 on only one side and 27% lost the sternocostal junctions of T7 on both sides and had only six ribs attached to the sternum (Table 3). Interestingly, we observed ectopic ossification centers in the sternum of *Btg2*-deficient animals, which resulted in supernumerary sternebrae in 20% of the mice (Fig 2C), probably due to the posterior homeotic transformation. On the other hand, the *Btg1*-deficient mice showed a reduced number of ossified sternebra(e), where the fourth and fifth sternebra lacked mineralization in 62% of mice, which was observed with much lower penetrance in *Btg2*^{-/-} (10%) and *Btg1*^{-/-};*Btg2*^{-/-} mice (27%) (Fig 2B–2D). During sternal development, ossification of the cartilage is inhibited at the site where the ribs contact the sternal rudiments.

Table 2. Mendelian inheritance in the offspring of *Btg1*; *Btg2* double knockout mice.

Breeding pairs	% +/+; +/+ exp./obs.	% +/+;+/- exp./obs.	% +/-; +/+ exp./obs.	% +/-;+/- exp./obs.	% +/-;-/- exp./obs.	% -/-; +/+ exp./obs.	% -/-;+/- exp./obs.	% -/-;-/- exp./obs.	P-value
<i>Btg1</i> ^{+/-} ; <i>Btg2</i> ^{+/-} x <i>Btg1</i> ^{+/-} ; <i>Btg2</i> ^{+/-}	12,5 / 6	12,5 / 19	12,5 / 14	12,5 / 22	6,25 / 11	12,5 / 10	12,5 / 5	12,5 / 6	<0.0001 (n = 118)
<i>Btg1</i> ^{+/-} ; <i>Btg2</i> ^{-/-} x <i>Btg1</i> ^{+/-} ; <i>Btg2</i> ^{-/-}	0 / 0	0 / 0	0 / 0	0 / 0	25 / 25	50 / 60	0 / 0	0 / 0	0.05 (n = 119)
<i>Btg1</i> ^{-/-} ; <i>Btg2</i> ^{+/-} x <i>Btg1</i> ^{-/-} ; <i>Btg2</i> ^{+/-}	0 / 0	0 / 0	0 / 0	0 / 0	0 / 0	0 / 0	25 / 56	50 / 44	<0.0001 (n = 40)
<i>Btg1</i> ^{-/-} ; <i>Btg2</i> ^{-/-} x <i>Btg1</i> ^{-/-} ; <i>Btg2</i> ^{-/-}	0 / 0	0 / 0	0 / 0	0 / 0	0 / 0	0 / 0	0 / 0	0 / 0	100 / 100 n.s.(n = 71)

Expected (exp.) mendelian inheritance and observed (obs.) inheritance after intercrossing compound *Btg1*;*Btg2* knockout animals. P-values of the mendelian ratios are calculated with the Chi-square test and are either significant if p <0.05 or not significant (n.s).

doi:10.1371/journal.pone.0131481.t002

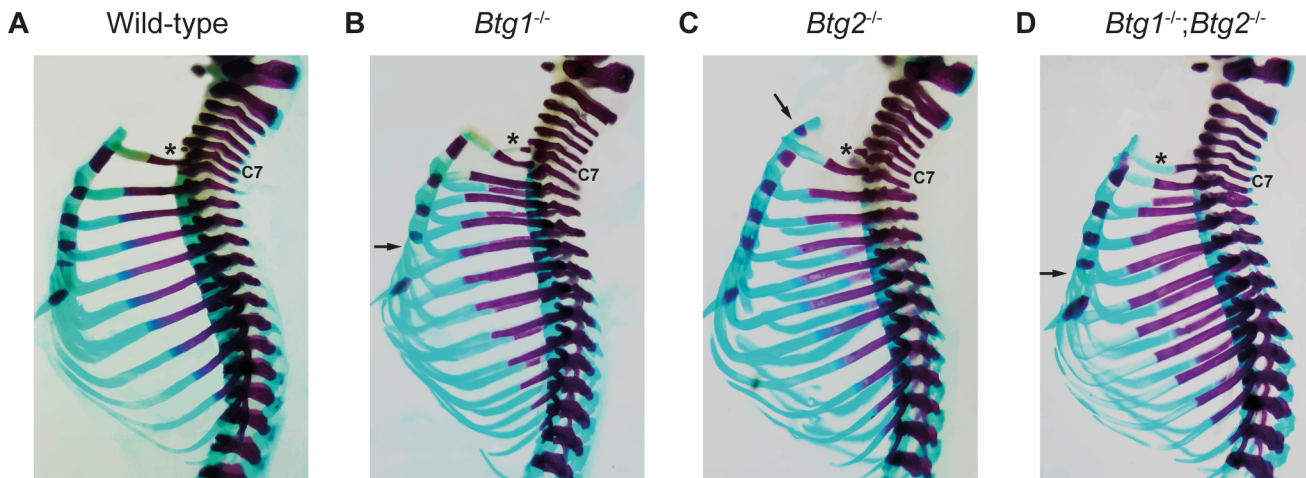


Fig 2. Skeletal abnormalities within the cervical-thoracic region in mice deficient for *Btg1* and *Btg2*. (A-D) Lateral view of the skeletons from 18.5 dpc wild-type, *Btg1*^{-/-}, *Btg2*^{-/-} and *Btg1*^{-/-};*Btg2*^{-/-} embryos, which were stained with alizarin red and alcian blue. (A-C) Wild-type *C57Bl6/J* mice show a rib anlage at C7 (indicated by asterisk), whereas *Btg1*^{-/-} and *Btg2*^{-/-} mice display a partial rib at C7 (indicated by asterisk). The extra formed T1 rib in *Btg1* knockout animal is fused to T2 rib. (D) *Btg1*^{-/-};*Btg2*^{-/-} double knockout mice display a full rib at C7 that is directly attached to the sternum (indicated by asterisk). (B and D) *Btg1*^{-/-} and *Btg1*^{-/-};*Btg2*^{-/-} embryos show often a reduction in the amount of ossified sternebrae (indicated by arrow) compared to wild-type. (C) *Btg2*^{-/-} deficient mice display occasionally an extra sternebra (indicated by arrow).

doi:10.1371/journal.pone.0131481.g002

Therefore, this process may become disturbed in the *Btg1*^{-/-} mice due to formation of inappropriate connections between the ribs and sternum. In addition, one *Btg1* knockout embryo showed an asymmetric pattern of ossification of the sternebrae, which was even more severe in another mouse lacking both *Btg1* and *Btg2* expression (Fig 3). Presumably, this type of sternal malformation, called crankshaft sternum, results from incorrect positioning of the attachment points of the costal cartilages on either sides of the sternal bar. In conclusion, these data show that both *Btg1* and *Btg2* regulate specification of cervical and thoracic vertebrae, whereas *Btg1* has a dominant function in regulating sternal ossification.

***Btg2* has a unique role in mediating homeotic transformation at the thoracic-lumbar region of the axial skeleton**

The rib pairs derived from T8 to T13 are termed “false ribs”, since they do not connect to the sternum. Instead, the T8 to T11 ribs form cartilaginous connections with the adjacent ribs, while T12 and T13 are considered floating ribs, since they form no connections to adjacent rib pairs (Fig 4A). Deletion of *Btg1* resulted in fourteen thoracic ribs in 62% of mice, as a consequence of the extra rib at C7, without any evidence of posterior transformation at the thoracic-lumbar junction (Fig 4B/Table 3). In contrast, mice deficient for *Btg2* displayed thirteen thoracic ribs as they acquired an extra rib at C7, while the thirteenth rib (T13) was often rudimentary or completely absent and acquired the identity of the first lumbar vertebra (L1) (Table 3). As a consequence, most *Btg2*^{-/-} mice showed only twelve thoracic ribs compared to thirteen in wild-type animals, and all *Btg2*^{-/-} mice displayed posterior homeotic transformation at the thoracic-lumbar junction (Fig 4C). Mice deficient for both *Btg1* and *Btg2* expression showed again normal numbers of thoracic ribs in 95% of the animals, since these mice displayed both C7 to T1 and T13 to L1 posterior transformations (Fig 4D/Table 3). These data demonstrate a unique function for *Btg2* in regulating the regional identity of vertebra at the thoracic to lumbar transition.

Table 3. Skeletal malformations in *Btg1*- and *Btg2*-deficient mice.

Vertebral transformation	WT(n = 18)	<i>Btg1</i> ^{-/-} (n = 21)	<i>Btg2</i> ^{-/-} (n = 20)	<i>Btg1</i> ^{-/-} ; <i>Btg2</i> ^{-/-} (n = 22)
Cervical region				
C7 rudimentary rib	13	8	13	0
C7 → T1 Fused (T1 to T2)	1	13	4	3
Full	0	0	3	18
Thoracic region				
Ossified Sternebrae				
#1	18	21	20	22
#2	18	21	20	22
#3	18	21	20	22
#4	18	20	18	22
#5	18	9	14	16
#6	0	0	4	0
Asymmetric sternum	0	1	0	1
Number of Ribs				
12	0	0	14	0
13	18	8	6	22
14	0	13	0	0
Ribs attached to sternum				
6	0	0	0	6
6/7	0	1	1	8
7	18	20	19	8
Lumbar region				
T13 → L1 partial	0	0	4	0
complete	0	0	16	21
Sacral region				
L5 → S1 partial	0	0	0	5
complete	0	0	0	10
L6 → S1 partial	0	5	0	1
complete	0	1	20	6

doi:10.1371/journal.pone.0131481.t003

Btg1 and Btg2 function are both required for specifying the vertebral identity at the lumbosacral region

Next, we examined the regional identity around the lumbosacral region of the axial skeleton in the *Btg1*^{-/-} and *Btg2*-deleted mice. While *Btg1* single knockout mice showed a partial or complete transformation of the sixth lumbar (L6) vertebra towards the identity of the first sacral vertebra (S1) with a penetrance of 29%, all *Btg2*^{-/-} mice displayed a complete transformation of L6 to S1 resulting in 6 lumbar vertebra due to the T13 to L1 transformation (Table 3). Interestingly, we observed a more severe phenotype in mice lacking both *Btg1* and *Btg2* expression, which showed complete transformation of L6 to S1 in 27% of mice, a partial transformation of L5 to S1 with a penetrance of 23% and a complete L5 to S1 transformation in 45% of the *Btg1*^{-/-};*Btg2*^{-/-} mice (Fig 5A–5C). As a consequence, mice with the L5 to S1 homeotic transformation had a reduction in the total amount of lumbar vertebrae. As a consequence of the L6 to S1 and L5 to S1 transformations, an anterior shift was observed in the position of the hindlimb, which is normally always connected to the position of the first sacral vertebra. Together these results demonstrate that there is a synergistic requirement for both *Btg1* and *Btg2* expression in specifying the correct identity of the lumbar vertebrae.

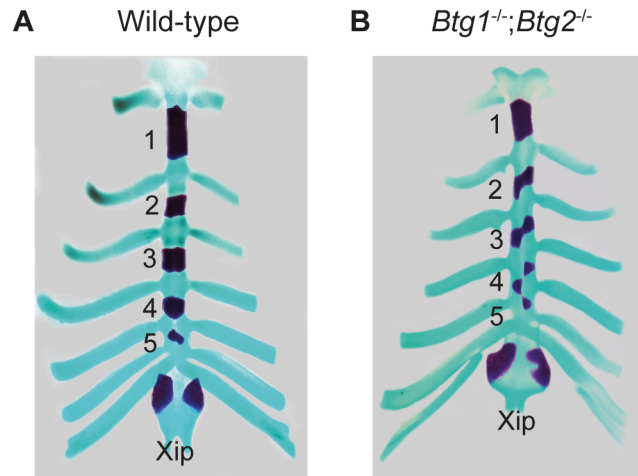


Fig 3. Targeted deletion of *Btg1* and *Btg2* results in malformation of the sternum. (A-B) Ventral view of the sternum with attached ribs of 18.5 dpc wild-type and *Btg1*^{-/-};*Btg2*^{-/-} embryos stained with alizarin red and alcian blue. Wild-type *C57BL6/J* mice display normal ossification of the five sternbrae, whereas an asymmetric pattern of ossification of the sternbrae is observed in mice lacking both *Btg1* and *Btg2* expression. The xiphoid process (Xip) of the sternum is not affected in *Btg1*^{-/-} and *Btg2*^{-/-} deficient mice.

doi:10.1371/journal.pone.0131481.g003

Discussion

The transcriptional cofactors *Btg1* and *Btg2* represent homologous proteins that regulate cellular proliferation and differentiation in different cell lineages. It was shown previously that *Btg2* is expressed in the presomitic mesoderm (PSM)-tail bud region of the mouse as well as in developing somites and that *Btg2* is involved in normal patterning of axial vertebrae [23]. However, a role for *Btg1* in regulating the development and regional specification of the mouse skeleton has not been reported so far. In this study, we used both *Btg1*^{-/-} and *Btg2*^{-/-} single and double deficient mice, to show that both genes play an essential role in conferring positional information along the anterior-posterior axis of the skeleton. Interbreeding of *Btg1* and *Btg2* homozygous knockout lines resulted in a smaller litter size and a non-mendelian inheritance pattern

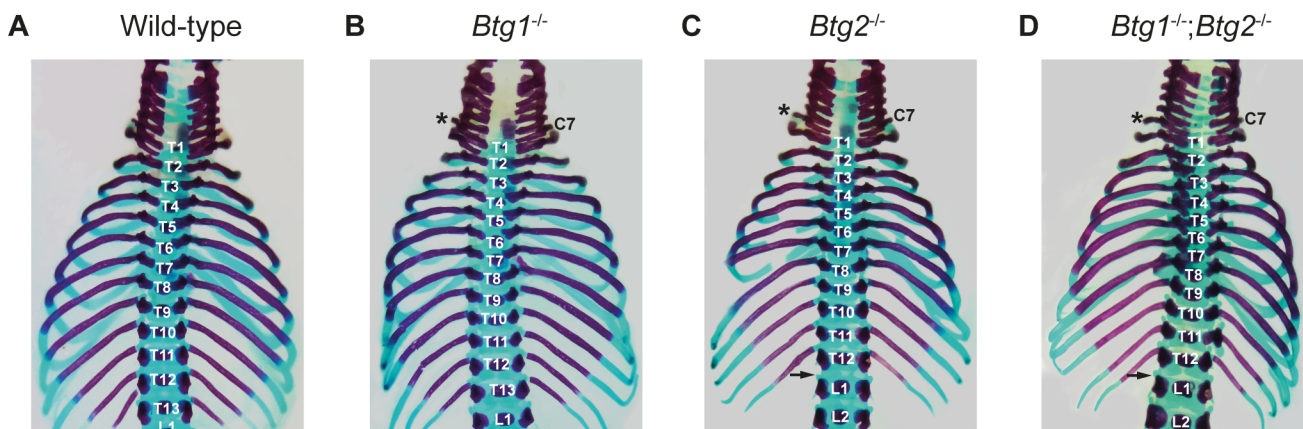


Fig 4. Posterior homeotic transformation of the thirteenth thoracic vertebra in mice deficient for *Btg2*. (A-D) Dorsal view of the cervicothoracic region of the skeleton in 18.5 dpc wild-type, *Btg1*^{-/-}, *Btg2*^{-/-} and *Btg1*^{-/-};*Btg2*^{-/-} embryos stained with alizarin red and alcian blue. (A-B) Wild-type *C57BL6/J* mice have thirteen thoracic ribs, while *Btg1*^{-/-} mice display fourteen ribs due to the extra extensive rib at C7. (D) Although the T13 rib is absent in *Btg1*^{-/-}; *Btg2*^{-/-} mice they still have thirteen thoracic ribs due to the C7 to T1 posterior transformation.

doi:10.1371/journal.pone.0131481.g004

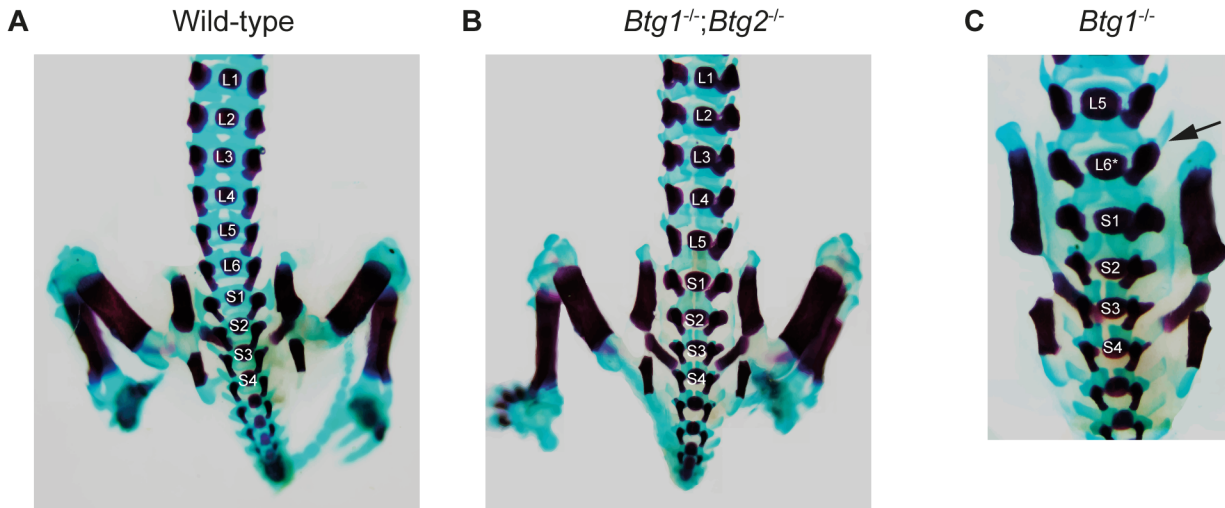


Fig 5. *Btg1*;*Btg2* double knockout mice display posterior homeotic transformation at the lumbo-sacral transition. Skeletal defects in 18.5 dpc wild-type, *Btg1*^{-/-} and *Btg1*^{-/-};*Btg2*^{-/-} embryos. (A-C) Dorsal view showing the lumbar-sacral regions. (B) *Btg1*^{-/-};*Btg2*^{-/-} mice frequently show five lumbar vertebrae compared to six in wild-type mice. (C) *Btg1*^{-/-} mice may show asymmetric L6 in which the right side (indicated by arrow) indicates a lumbar vertebra and the left side a sacral vertebra.

doi:10.1371/journal.pone.0131481.g005

for the *Btg1* single knockout crosses and the *Btg2* knockout allele in the compound crosses. *Btg1* and *Btg2* are separately implicated in regulating patterning of the lower cervical region, but the combined action of both genes is required for specifying the correct identity of the seventh cervical and the sixth lumbar vertebra. On the other hand, *Btg2* expression appears to be more uniquely involved in the specification of the vertebra at the thoracic-lumbar junction (Fig 6).

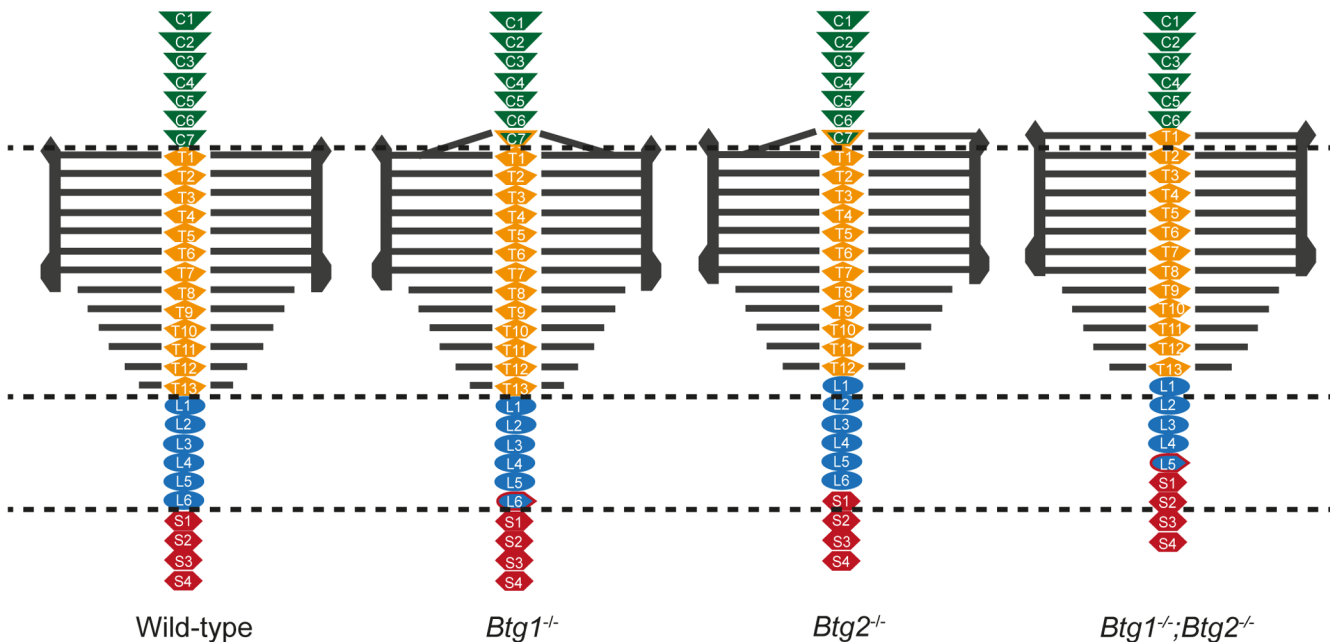


Fig 6. Overview of the skeletal phenotypes in *Btg1*- and *Btg2*-deficient mice. Axial vertebrae are indicated by different colors: green (cervical), yellow (thoracic), blue (lumbar) and red (sacral). The thoracic ribs are indicated by the grey horizontal lines, of which T1-T7 form sternocostal junctions with the sternum. *Btg1*^{-/-} and *Btg2*^{-/-} deficient mice display C7 to T1 posterior transformation, while *Btg1*^{-/-} mice show also partial or complete L6 to S1. *Btg2*^{-/-} mice display in most cases T13 to L1 and complete L6 to S1 transformations. *Btg1*^{-/-};*Btg2*^{-/-} double knockout animals display a more pronounced phenotype with C7 to T1, T13 to L1 and L6 to S1 homeotic transformations.

doi:10.1371/journal.pone.0131481.g006

Our studies demonstrate that deletion of both *Btg1* and *Btg2* results in an aggravated phenotype, revealing a synergistic effect upon a combined loss of these genes. An extra rib at the seventh cervical vertebra was observed with a low incidence in the *Btg2* knockout mice, and posterior homeotic transformation at this position was more pronounced in the absence of *Btg1* expression. In 95% of the *Btg1*^{-/-};*Btg2*^{-/-} double knockout mice a complete C7 to T1 transformation was observed, arguing that the action of both genes is required for instructing the proper identity of the seventh cervical vertebra. In agreement with previous studies, we found that *Btg2*^{-/-} mice displayed homeotic transformation of the thirteenth thoracic vertebra. In contrast, *Btg1*-deficiency had no significant impact on regulating the identity of this last thoracic vertebra, which was also evident from the fact that the double knockout showed a phenotype similar to the *Btg2*^{-/-} mice at the thoracic-lumbar junction. Both *Btg1*- and *Btg2*-deficient mice displayed partial or complete homeotic transformation of the sixth lumbar vertebra towards the first sacral vertebra (L6 to S1), and this phenotype was even more severe in the *Btg1*^{-/-};*Btg2*^{-/-} double knockout mice. Thus, *Btg1* and *Btg2* display both unique and overlapping functions along the anterior-posterior axis in regulating specification of vertebral identity.

Deficiency of *Btg1* resulted in reduced ossification of the distal sternebra(e) as a consequence of delayed ossification within the sternal bands. We also observed abnormal ossification of the sternum where the corresponding costal cartilages invariably inserted into the sternum at different levels at the two sides leading to an asymmetric sternum, known as “crankshaft sternum” [29]. Endochondral bone ossification is regulated by several different signaling pathways, including the action of Runx1 and Runx2 transcription factors [30, 31]. However, it remains to be established whether these defects are primarily the consequence of endochondral ossification defects, or occur secondary to inappropriate connections made between the rib ends and the sternum.

Previously, *Btg2* has been considered to regulate skeletal development by modulating BMP/Smad signaling, but the skeletal abnormalities observed in the *Btg1*- and *Btg2*-deleted mice are more reminiscent of the phenotype of several knockout mouse models deficient in Polycomb group genes (PcG), including *Bmi1*, *Mel18* and *M33* [32–35]. In addition, similar abnormalities have been described for mice deficient in *E2f6* and the spliceosomal protein *Sf3b1*, which are known to associate with a number of PcG proteins. The interaction of PcG proteins with *Sf3b1* and *E2f6* is essential for the PcG-mediated repression of *Hox* genes [36–40]. Compared to single PcG mutants, the *Bmi1*^{-/-};*M33*^{-/-} and *E2f6*^{-/-};*Bmi1*^{-/-} double knockout mice reveal extended skeletal transformations [35, 41], due to enhanced deregulation and loss of direct transcriptional control of the *Hox* genes.

Taken together, our data show that *Btg1* and *Btg2* play an important role in anterior-posterior patterning along the vertebral column and both genes fulfill largely overlapping functions in specifying the correct positional identity.

Acknowledgments

The authors thank WIL Research for lending their expertise on defining skeletal malformations in *Btg1* and *Btg2* knockout embryos.

This work was funded by “Kinderen Kankervrij” (KiKa; project number 77).

Author Contributions

Conceived and designed the experiments: ET PMH FNVL BS. Performed the experiments: ET DvIS FvO. Analyzed the data: ET DvIS BS. Contributed reagents/materials/analysis tools: FT. Wrote the paper: ET PMH FNVL BS.

References

1. Dubrulle J, Pourquie O. Coupling segmentation to axis formation. *Development*. 2004; 131(23):5783–93. Epub 2004/11/13. PMID: [15539483](#)
2. Hirsinger E, Jouve C, Dubrulle J, Pourquie O. Somite formation and patterning. *International review of cytology*. 2000; 198:1–65. Epub 2000/05/11. PMID: [10804460](#)
3. Krumlauf R. Hox genes in vertebrate development. *Cell*. 1994; 78(2):191–201. Epub 1994/07/29. PMID: [7913880](#)
4. Duboule D. The rise and fall of Hox gene clusters. *Development*. 2007; 134(14):2549–60. Epub 2007/06/08. PMID: [17553908](#)
5. Duboule D, Dolle P. The structural and functional organization of the murine HOX gene family resembles that of *Drosophila* homeotic genes. *The EMBO journal*. 1989; 8(5):1497–505. Epub 1989/05/01. PMID: [2569969](#)
6. Graham A, Papalopulu N, Krumlauf R. The murine and *Drosophila* homeobox gene complexes have common features of organization and expression. *Cell*. 1989; 57(3):367–78. Epub 1989/05/05. PMID: [2566383](#)
7. Alexander T, Nolte C, Krumlauf R. Hox genes and segmentation of the hindbrain and axial skeleton. *Annual review of cell and developmental biology*. 2009; 25:431–56. Epub 2009/07/07. doi: [10.1146/annurev.cellbio.042308.113423](#) PMID: [19575673](#)
8. Mallo M, Wellik DM, Deschamps J. Hox genes and regional patterning of the vertebrate body plan. *Developmental biology*. 2010; 344(1):7–15. Epub 2010/05/04. doi: [10.1016/j.ydbio.2010.04.024](#) PMID: [20435029](#)
9. Tschopp P, Duboule D. A genetic approach to the transcriptional regulation of Hox gene clusters. *Annual review of genetics*. 2011; 45:145–66. Epub 2011/11/09. doi: [10.1146/annurev-genet-102209-163429](#) PMID: [22060042](#)
10. Cernilogar FM, Orlando V. Epigenome programming by Polycomb and Trithorax proteins. *Biochemistry and cell biology = Biochimie et biologie cellulaire*. 2005; 83(3):322–31. Epub 2005/06/17. PMID: [15959558](#)
11. Grimaud C, Negre N, Cavalli G. From genetics to epigenetics: the tale of Polycomb group and trithorax group genes. *Chromosome research: an international journal on the molecular, supramolecular and evolutionary aspects of chromosome biology*. 2006; 14(4):363–75. Epub 2006/07/06.
12. Mallo M, Vinagre T, Carapuco M. The road to the vertebral formula. *The International journal of developmental biology*. 2009; 53(8–10):1469–81. Epub 2009/02/28. doi: [10.1387/ijdb.072276mm](#) PMID: [19247958](#)
13. Benazeraf B, Pourquie O. Formation and segmentation of the vertebrate body axis. *Annual review of cell and developmental biology*. 2013; 29:1–26. Epub 2013/07/03. doi: [10.1146/annurev-cellbio-101011-155703](#) PMID: [23808844](#)
14. Rouault JP, Falette N, Guehenneux F, Guillot C, Rimokh R, Wang Q, et al. Identification of BTG2, an antiproliferative p53-dependent component of the DNA damage cellular response pathway. *Nature genetics*. 1996; 14(4):482–6. Epub 1996/12/01. PMID: [8944033](#)
15. Winkler GS. The mammalian anti-proliferative BTG/Tob protein family. *Journal of cellular physiology*. 2010; 222(1):66–72. Epub 2009/09/12. doi: [10.1002/jcp.21919](#) PMID: [19746446](#)
16. Sun Q, Hang M, Guo X, Shao W, Zeng G. Expression and significance of miRNA-21 and BTG2 in lung cancer. *Tumour biology: the journal of the International Society for Oncodevelopmental Biology and Medicine*. 2013; 34(6):4017–26. Epub 2013/07/17.
17. Zhao Y, Gou WF, Chen S, Takano Y, Xiu YL, Zheng HC. BTG1 expression correlates with the pathogenesis and progression of ovarian carcinomas. *International journal of molecular sciences*. 2013; 14(10):19670–80. Epub 2013/10/03. doi: [10.3390/ijms141019670](#) PMID: [24084718](#)
18. Kuiper RP, Schoenmakers EF, van Reijmersdal SV, Hehir-Kwa JY, van Kessel AG, van Leeuwen FN, et al. High-resolution genomic profiling of childhood ALL reveals novel recurrent genetic lesions affecting pathways involved in lymphocyte differentiation and cell cycle progression. *Leukemia*. 2007; 21(6):1258–66. Epub 2007/04/20. PMID: [17443227](#)
19. Sheng SH, Zhao CM, Sun GG. BTG1 expression correlates with the pathogenesis and progression of breast carcinomas. *Tumour biology: the journal of the International Society for Oncodevelopmental Biology and Medicine*. 2014; 35(4):3317–26. Epub 2013/11/26.
20. Mullighan CG, Goorha S, Radtke I, Miller CB, Coustan-Smith E, Dalton JD, et al. Genome-wide analysis of genetic alterations in acute lymphoblastic leukaemia. *Nature*. 2007; 446(7137):758–64. Epub 2007/03/09. PMID: [17344859](#)

21. Lohr JG, Stojanov P, Lawrence MS, Auclair D, Chapuy B, Sougnez C, et al. Discovery and prioritization of somatic mutations in diffuse large B-cell lymphoma (DLBCL) by whole-exome sequencing. *Proceedings of the National Academy of Sciences of the United States of America*. 2012; 109(10):3879–84. Epub 2012/02/22. doi: [10.1073/pnas.1121343109](https://doi.org/10.1073/pnas.1121343109) PMID: [22343534](https://pubmed.ncbi.nlm.nih.gov/22343534/)
22. Morin RD, Mendez-Lago M, Mungall AJ, Goya R, Mungall KL, Corbett RD, et al. Frequent mutation of histone-modifying genes in non-Hodgkin lymphoma. *Nature*. 2011; 476(7360):298–303. Epub 2011/07/29. doi: [10.1038/nature10351](https://doi.org/10.1038/nature10351) PMID: [21796119](https://pubmed.ncbi.nlm.nih.gov/21796119/)
23. Park S, Lee YJ, Lee HJ, Seki T, Hong KH, Park J, et al. B-cell translocation gene 2 (*Btg2*) regulates vertebral patterning by modulating bone morphogenetic protein/smad signaling. *Molecular and cellular biology*. 2004; 24(23):10256–62. Epub 2004/11/16. PMID: [15542835](https://pubmed.ncbi.nlm.nih.gov/15542835/)
24. Prevot D, Voeltzel T, Birot AM, Morel AP, Rostan MC, Magaud JP, et al. The leukemia-associated protein *Btg1* and the p53-regulated protein *Btg2* interact with the homeoprotein *Hoxb9* and enhance its transcriptional activation. *The Journal of biological chemistry*. 2000; 275(1):147–53. Epub 2000/01/05. PMID: [10617598](https://pubmed.ncbi.nlm.nih.gov/10617598/)
25. Alharbi RA, Pettengell R, Pandha HS, Morgan R. The role of HOX genes in normal hematopoiesis and acute leukemia. *Leukemia*. 2013; 27(5):1000–8. Epub 2012/12/06. doi: [10.1038/leu.2012.356](https://doi.org/10.1038/leu.2012.356) PMID: [23212154](https://pubmed.ncbi.nlm.nih.gov/23212154/)
26. Radulovic V, de Haan G, Klauke K. Polycomb-group proteins in hematopoietic stem cell regulation and hematopoietic neoplasms. *Leukemia*. 2013; 27(3):523–33. Epub 2012/12/22. doi: [10.1038/leu.2012.368](https://doi.org/10.1038/leu.2012.368) PMID: [23257781](https://pubmed.ncbi.nlm.nih.gov/23257781/)
27. Casaca A, Santos AC, Mallo M. Controlling Hox gene expression and activity to build the vertebrate axial skeleton. *Developmental dynamics: an official publication of the American Association of Anatomists*. 2014; 243(1):24–36. Epub 2013/07/03.
28. Farioli-Vecchioli S, Micheli L, Sarauili D, Ceccarelli M, Cannas S, Scardigli R, et al. *Btg1* is Required to Maintain the Pool of Stem and Progenitor Cells of the Dentate Gyrus and Subventricular Zone. *Frontiers in neuroscience*. 2012; 6:124. Epub 2012/09/13. doi: [10.3389/fnins.2012.00124](https://doi.org/10.3389/fnins.2012.00124) PMID: [22969701](https://pubmed.ncbi.nlm.nih.gov/22969701/)
29. Horan GS, Wu K, Wolgemuth DJ, Behringer RR. Homeotic transformation of cervical vertebrae in *Hoxa-4* mutant mice. *Proceedings of the National Academy of Sciences of the United States of America*. 1994; 91(26):12644–8. Epub 1994/12/20. PMID: [7809093](https://pubmed.ncbi.nlm.nih.gov/7809093/)
30. Ding M, Lu Y, Abbassi S, Li F, Li X, Song Y, et al. Targeting *Runx2* expression in hypertrophic chondrocytes impairs endochondral ossification during early skeletal development. *Journal of cellular physiology*. 2012; 227(10):3446–56. Epub 2012/01/10. doi: [10.1002/jcp.24045](https://doi.org/10.1002/jcp.24045) PMID: [22223437](https://pubmed.ncbi.nlm.nih.gov/22223437/)
31. Soung do Y, Talebian L, Matheny CJ, Guzzo R, Speck ME, Lieberman JR, et al. *Runx1* dose-dependently regulates endochondral ossification during skeletal development and fracture healing. *Journal of bone and mineral research: the official journal of the American Society for Bone and Mineral Research*. 2012; 27(7):1585–97. Epub 2012/03/21.
32. van der Lugt NM, Domen J, Linders K, van Roon M, Robanus-Maandag E, te Riele H, et al. Posterior transformation, neurological abnormalities, and severe hematopoietic defects in mice with a targeted deletion of the *bmi-1* proto-oncogene. *Genes & development*. 1994; 8(7):757–69. Epub 1994/04/01.
33. Core N, Bel S, Gaunt SJ, Aurrand-Lions M, Pearce J, Fisher A, et al. Altered cellular proliferation and mesoderm patterning in Polycomb-M33-deficient mice. *Development*. 1997; 124(3):721–9. Epub 1997/02/01. PMID: [9043087](https://pubmed.ncbi.nlm.nih.gov/9043087/)
34. Akasaka T, van Lohuizen M, van der Lugt N, Mizutani-Koseki Y, Kanno M, Taniguchi M, et al. Mice doubly deficient for the Polycomb Group genes *Mel18* and *Bmi1* reveal synergy and requirement for maintenance but not initiation of Hox gene expression. *Development*. 2001; 128(9):1587–97. Epub 2001/04/06. PMID: [11290297](https://pubmed.ncbi.nlm.nih.gov/11290297/)
35. Bel S, Core N, Djabali M, Kieboom K, Van der Lugt N, Alkema MJ, et al. Genetic interactions and dosage effects of Polycomb group genes in mice. *Development*. 1998; 125(18):3543–51. Epub 1998/08/26. PMID: [9716520](https://pubmed.ncbi.nlm.nih.gov/9716520/)
36. Storre J, Elsasser HP, Fuchs M, Ullmann D, Livingston DM, Gaubatz S. Homeotic transformations of the axial skeleton that accompany a targeted deletion of *E2f6*. *EMBO reports*. 2002; 3(7):695–700. Epub 2002/07/09. PMID: [12101104](https://pubmed.ncbi.nlm.nih.gov/12101104/)
37. Attwooll C, Lazzarini Denchi E, Helin K. The E2F family: specific functions and overlapping interests. *The EMBO journal*. 2004; 23(24):4709–16. Epub 2004/11/13. PMID: [15538380](https://pubmed.ncbi.nlm.nih.gov/15538380/)
38. Trimarchi JM, Fairchild B, Wen J, Lees JA. The E2F6 transcription factor is a component of the mammalian *Bmi1*-containing polycomb complex. *Proceedings of the National Academy of Sciences of the United States of America*. 2001; 98(4):1519–24. Epub 2001/02/15. PMID: [11171983](https://pubmed.ncbi.nlm.nih.gov/11171983/)
39. Isono K, Mizutani-Koseki Y, Komori T, Schmidt-Zachmann MS, Koseki H. Mammalian polycomb-mediated repression of Hox genes requires the essential spliceosomal protein *Sf3b1*. *Genes & development*. 2005; 19(5):536–41. Epub 2005/03/03.

40. Ogawa H, Ishiguro K, Gaubatz S, Livingston DM, Nakatani Y. A complex with chromatin modifiers that occupies E2F- and Myc-responsive genes in G0 cells. *Science*. 2002; 296(5570):1132–6. Epub 2002/05/11. PMID: [12004135](#)
41. Courel M, Friesenhahn L, Lees JA. E2f6 and Bmi1 cooperate in axial skeletal development. *Developmental dynamics: an official publication of the American Association of Anatomists*. 2008; 237(5):1232–42. Epub 2008/03/28.